Dynamics of Polymer/Metal Nanocomposite Films at Short Times As Studied by X-ray Standing Waves

Rodney S. Guico,[†,‡] Suresh Narayanan,[†] Jin Wang,[†] and Kenneth R. Shull*[,‡]

Experimental Facilities Division, Advanced Photon Source, Argonne National Laboratory, Argonne, Illinois 60439, and Department of Materials Science and Engineering, Northwestern University, Evanston, Illinois 60208

Received July 2, 2004; Revised Manuscript Received August 6, 2004

ABSTRACT: X-ray standing waves generated by total external reflection from a silver mirror were used to monitor the mobility of metal particles in ultrathin polymer matrices with subnanometer spatial resolution in the direction perpendicular to the film surface. The particular model system consisted of gold nanoparticles deposited onto poly(*tert*-butyl acrylate) (PtBA) by thermal evaporation. Particles remained at the free surface of a PtBA film during annealing treatments above the polymer glass transition temperature but were able to diffuse when a second polymer layer was added to create sandwich samples with a buried gold layer. In these sandwich samples the gold distribution broadened with time and moved toward the polymer layer with the highest mobility. The polymer mobility is affected by the molecular weight of the polymer itself and by the substrate with which the layer is in contact. Values of the gold particle diffusion coefficients obtained from the broadening of the distribution are coupled to the terminal relaxation time of the polymer. An effective step size, defined as the average distance a gold particle moves within the relaxation time of the polymer, is equal to a few percent of the tube diameter.

Introduction

Dispersions of nanoscale, inorganic nanoparticles are of great scientific and technical interest because of their novel electronic, magnetic, and photonic properties. Ordered polymeric materials such as diblock copolymers are particularly useful as matrix materials for these dispersions because of the ability to control the size and distribution of the particles.[1−6] The formation of the structures is a complex process controlled by thermodynamic and kinetic factors. The initial response of the metal particles is to conform to the preexisting morphology of the diblock copolymer template by diffusive motions of the metal particles over short distances, followed by particle coalescence. Continued particle coalescence and reorganization of the block copolymer in response to the presence of the metal occur at longer times, thereby destroying the templated morphology. Since these processes take place far from equilibrium conditions, effective use of these ordering mechanisms requires an understanding of the dynamics of metal particle motion on time scales that are comparable to the characteristic relaxation time of the underlying polymer template. In this regard, dilute particles in homopolymer matrices are simpler model systems for studying the particle dynamics at the early stages. In these systems, the relevant length scale is the entanglement spacing, ξ (typically several nanometers), and the relevant relaxation time corresponds to the entanglement lifetime, τ. To understand the diffusion and transport properties of the particles on these length and time scales, experimental probes that are capable of detecting particle motions in situ with subnanometer spatial resolution are required. While a number of experimental studies of metal particle diffusion in polymer matrices have been reported,[7−9] their spatial resolution has not been sufficient to elucidate motion of the particles on time scales comparable to the relaxation time of the entanglement network.

In this paper, we describe a model metal particle/polymer system that is ideally suited for studying the dynamic properties of metal particle dispersions on these short time scales with unprecedented spatial resolution. The sample is a gold/poly(*tert*-butyl acrylate) (PtBA) nanocomposite, and our experimental technique involves the use of X-ray standing waves (XSWs) generated by total external reflection (TER). PtBA is an amorphous homopolymer with stability against photooxidation and an easily accessible glass transition temperature (T_g) of 49 °C.[10,11] Monodisperse polymers with weight-average molecular weights of 100 000, 185 000, or 350 000 were used in these studies.

Experimental Section

Materials. Samples of anionically polymerized poly(*tert*-butyl acrylate)[12,13] with weight-average molecular weights, M, ranging from 100 000 to 350 000 were used in these experiments. The polydispersity index for each of the polymer samples was less than 1.2. Frequency-dependent dynamic shear moduli for a polymer with $M = 350\,000$ were measured at temperatures ranging from 75 to 140 °C, using a Rheometrics Scientific ARES rheometer.

To prepare the thin film nanocomposite samples for the X-ray studies, float-glass substrates were first placed in a thermal evaporation system and coated with thin layers of Cr (50 Å) and Ag (500 Å). Upon removal from the evaporation chamber, PtBA films (thickness ≈ 400 Å) were immediately coated onto the silver layer by spin-casting from a butanol solution. These samples were then placed back in the evaporation chamber, and an ultrathin layer of gold was deposited onto the PtBA surface. The total coverage of the gold layer, evaporated at a rate of 0.3 Å/s, was measured during deposition using a quartz-crystal monitor and was equivalent to a continuous layer with a thickness of 4 Å ($z^* = 4$ Å). Because the polymer−metal interaction is much weaker than that between the metal atoms, evaporation of noble metals such as gold onto polymer surfaces leads to the formation of

[†] Argonne National Laboratory.
[‡] Northwestern University.

10.1021/ma0486593 CCC: $27.50
Published on Web 10/01/2004

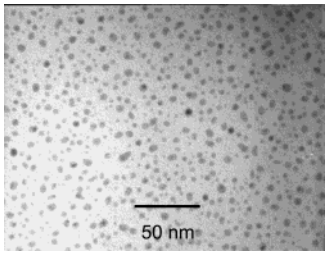

Figure 1. TEM image of the gold particle morphology.

nanoclusters via a Volmer−Weber growth mode.[14] Therefore, this ultrathin layer of gold exists as a two-dimensional distribution of individual particles. In most cases, a second PtBA layer of equivalent thickness was floated onto a water bath and picked up on top of the gold particle layer to create "sandwich" samples in which the gold layer was buried between two PtBA films with similar thicknesses. Some experiments were also performed on "open-face" samples, where the second PtBA layer was not added.

Nanocomposite samples for characterization by transmission electron microscopy (TEM) were produced in a similar manner. In these cases thin PtBA films with a thickness of 1100 Å were spun-cast onto clean glass slides or freshly cleaved mica substrates. The samples were dried in air to remove any residual solvent. Gold was thermally evaporated onto these dried films, and the films were then scribed into small pieces and floated onto a water bath. Carbon-coated TEM grids were used to capture the films for further study, and these were allowed to dry in air again for at least 12 h. The morphology of the gold particle layer is illustrated by the TEM image in Figure 1.

X-ray Standing Wave Measurements. To study nanoscale interactions, a surface and interface sensitive probe was needed that was applicable to the dilute nanoparticle system. The X-ray standing wave (XSW) technique, developed in the 1960s, has been used primarily for probing heavy atoms in and on perfect single crystals with subangstrom spatial resolution.[15−17] This type of standing waves is created by Bragg diffraction from a single crystal, so the period of the standing wave is fixed to the lattice spacing. The discovery of XSWs generated by total external reflection (TER) above an X-ray mirror surface has made it possible to study particles in polymer matrices on larger length scales of tens to hundreds of angstroms, which is well suited to our sample geometry.[18,19] In this technique an X-ray beam with a wavelength of λ impinges on a mirror surface at an angle, θ, below the critical angle, θ_c, of the mirror. The incident and reflected X-rays coherently interfere to create XSWs above the silver mirror with a period of $d = \lambda/(2 \sin \theta)$. The electric field intensity, I, can be calculated over the entire sample at any given angle from the following expression:

$$I = |E_0|^2(1 + R + 2R^{1/2} \cos[\phi^R - 2\pi q_z z]) \qquad (1)$$

where E_0 is the incident electric field amplitude, R is the reflectivity, ϕ^R is the phase shift of the reflected beam, and q_z is the magnitude of the wave-vector transfer in the z direction, given by $q_z = 2\pi \sin \theta/\lambda$. At scattering angles that are well below the critical angle of the mirror, the first antinode of the standing wave exists far above the mirror surface. As the incident angle is increased toward θ_c (5.08 mrad in our case), the first antinode moves toward the mirror surface like a collapsing bellows. At exactly the critical angle, the first antinode is coincident with the silver mirror, and the standing wave is given by a critical period $d_c = \lambda/(2 \sin \theta_c)$. In our experiment the wavelength, λ, is 1.0247 Å and $d_c = 100$ Å, so approximately four standing wave oscillations would pass through a heavy atom layer (gold) positioned about 375 Å above the silver mirror surface. A high-Z material, silver, was chosen as a mirror due to its large electron density and, consequently, its small critical period. When the X-ray energy is above the absorption edge of the heavy atom layer residing above the mirror surface, the photoelectric effect at the center of the atoms creates a characteristic fluorescence signal. This signal, which peaks when the planes of maximum electric field intensity pass through the marker layer, can serve as a probe of the distribution and position of the gold particles above the silver mirror. The electric field intensity, as well as the reflectivity, can be calculated using Parratt's recursive formalism.[20] The fluorescence yield, Y, as a function of θ and the annealing time, t, is given by the following integral:

$$Y(\theta,t) \propto \int I(z,\theta)\, \phi(z,t)\, dz \qquad (2)$$

where ϕ is the gold particle volume fraction and z is the distance above the mirror surface. A Gaussian form is assumed for the particle distribution:

$$\phi(z,t) = (2\pi)^{-1/2}(z^*/\sigma) \exp([z - z_0(t)]^2/\{2[\sigma(t)]^2\}) \qquad (3)$$

where σ is the Gaussian width of the distribution and z_0 is the mean position of the gold layer above the mirror surface.

The XSW experiments were carried out at the 1-BM beamline at the Advanced Photon Source at Argonne National Laboratory. The X-rays were monrochromated to an energy of 12.1 keV (λ = 1.024 Å), optimized for exciting gold L fluorescence. The beam size at the sample was 2.25 mm (horizontal) × 0.045 mm (vertical), with a flux density of 5×10^8 photons/(s mm^2). Such a flux density was chosen to minimize the radiation damage to the polymer. The samples were annealed in a temperature-controlled chamber filled with He gas to reduce the attenuation and to reduce the probability of radiation damage to the polymer films. A NaI scintillation detector was used for collecting the reflectivity data, while a Ge solid-state detector collected the fluorescence signal.

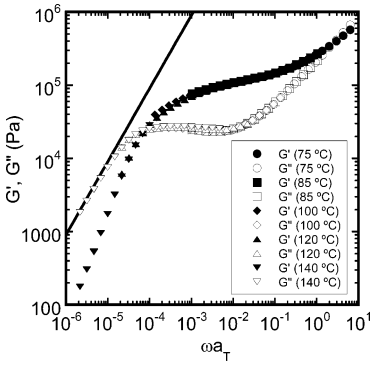

Figure 2. Master plot of the storage and loss moduli for PtBA with a molecular weight of 350 000, as measured by oscillatory shear rheometry. Data were shifted to a reference temperature of 63 °C by using the shift factors plotted in Figure 3. The solid line corresponds to a Newtonian viscosity of 9×10^8 Pa s.

Results and Discussion

Rheometry. The magnitude of the complex shear modulus is plotted as a function of the reduced frequency in Figure 2 for a PtBA homopolymer with M = 350 000. Data were obtained at temperatures of 75, 85, 100, 120, and 140 °C. The temperature shift factors used to obtain the master plot are shown in Figure 3, along with temperature shift factors obtained previously by Cole et al. at temperatures extending to 180 °C.[11] The solid line in Figure 3 represents a fit to the Vogel equation:

$$\log(a_T) = A + \frac{B}{T - T_\infty} \qquad (4)$$

with $A = -8.94$, $B = 706$, and $T_\infty = -16$ °C. This value

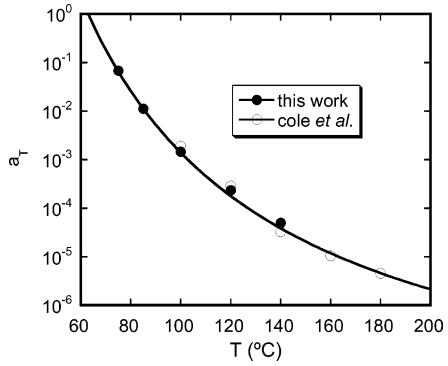

Figure 3. Fit to the Vogel equation for obtaining shift factors from the rheology data. The solid line is obtained using eq 4, with $A = -8.94$, $B = 706$, and $T_\infty = -16$. The data from Figure 2 were combined with data from Cole et al. (100 °C < T < 180 °C) (ref 11), and all of the data were shifted to give $a_T = 1$ at the reference temperature of 63 °C.

for T_∞ is 65 °C less than the measured glass transition temperature of 49 °C. The value of −8.94 for A was chosen so that $a_T = 1$ at a reference temperature of 63 °C.

The rheological data can be used to determine the temperature dependence of the terminal relaxation time, τ, for the polymers. In the low-frequency, terminal regime, G'' is proportional to ω, with a slope given by the zero shear viscosity, η_0. The solid line in Figure 2 corresponds to a material with $\eta_0 = 9 \times 10^8$ Pa s. Because η_0 has the same temperature dependence as the shift factor, a_T, and because η_0 is known to scale with the 3.4 power of the polymer molecular weight for entangled polymers, we can use the data in Figures 2 and 3 to develop the following expression for the zero shear viscosity of monodisperse PtBA homopolymers in the entangled regime:

$$\eta_0\,(\text{Pa s}) = \frac{9 \times 10^8}{(350000)^{3.4}} M^{3.4} a_T = 1.45 \times 10^{-19} M^{3.4} \exp(1626/(T + 16)) \quad (5)$$

with M in g/mol and T in °C. For entangled polymers, η_0 is given approximately by τG_n^0, where G_n^0 is the plateau modulus. An estimate of 10^5 Pa is obtained for G_n^0 by using the value of G' at the frequency corresponding to the inflection point in G''. The molecular weight and temperature dependence of the terminal relaxation time for monodisperse, entangled PtBA can therefore be expressed as follows:

$$\tau\,(\text{s}) = 1.45 \times 10^{-24} M^{3.4} \exp(1626/(T + 16)) \quad (6)$$

with T expressed in °C. The terminal relaxation time for $M = 350\,000$ at the reference temperature of 63 °C is 9000 s. The terminal relaxation time for this polymer at higher temperature is obtained by multiplying this value by the temperature shift factors plotted in Figure 3.

Equation 4 is in quantitative agreement with the previously published relationship given by Cole et al.,[11] even though the present value of −16 °C for T_∞ differs from the value of −10 °C that was used in the previous study. Both values of T_∞ adequately describe the data in the previous temperature range (100−180 °C), but the lower value of T_∞ is needed in order to describe the temperature shift factors at the low end of the temperature range. Equations 5 and 6 are valid over the full range of measured temperatures (75−180 °C), but some care needs to be taken when using these values to draw conclusions from some of the XSW results obtained at temperatures below 75 °C.

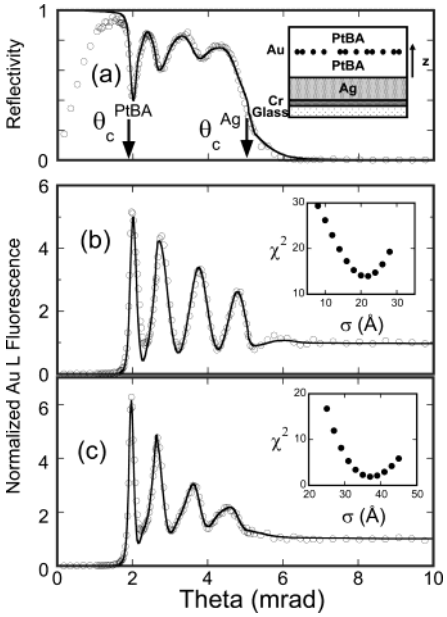

Figure 4. Reflectivity (a) and fluorescence (b) profiles for a 400 Å symmetric sandwich with $M = 350\,000$ at room temperature. The sample geometry is shown schematically in the inset of (a). The fluorescence profile of the sample annealed at 85 °C for 60 min is shown in (c). The solid lines are fits to the experimental data (open circles). The insets in (b) and (c) show the χ^2-fitting of the Gaussian width, σ, for both profiles.

X-ray Standing Wave Results. The results of the XSW measurements are shown in Figure 4 for a symmetric sandwich sample with a 375 Å layer of PtBA with $M = 350\,000$ on either side of the gold particles. This figure shows the angular dependence of the experimental and fitted reflectivity (a) and fluorescence profile (b) at ca. 30 °C. In the reflectivity curve, the interference between the reflected X-rays produces modulations in the region between the critical angles of PtBA (≈2 mrad) and the silver mirror (≈5.2 mrad), revealing the thickness of the PtBA layers as well as the approximate distance of the gold particle layer from the Ag mirror. In the fluorescence profile, approximately four peaks are seen in the same angular region, consistent with the simple argument that accounts for the 100 Å critical period of the Ag mirror. The fluorescence profiles shown here have been normalized to the same area illuminated by the X-ray beam. In Figure 4b, σ and z_0 were determined by performing χ^2-minimization during the fitting procedure. At ca. 30 °C, $\sigma = 17$ Å and $z_0 = 366$ Å. The value of σ in these unannealed samples is consistent with the particle size measured with TEM. Since the electric field intensity is a function of the reflection from each layer, refinement of the fluorescence fit was done in conjunction with fitting of the reflectivity data. Then, the nanocomposite sample was annealed at various temperatures above T_g. Measurements were taken in situ during the anneal with each reflection curve and fluorescence profile lasting no longer than 3 min and occurring at 30 min intervals to avoid radiation damage. The results from the annealed sample at 85 °C are shown in Figure 4c. After 60 min at 85 °C, there are distinct differences from the profile measured at 30 °C, especially in the angular range of interest (≈3−5 mrad). In the case of the sandwich nanocomposite, not

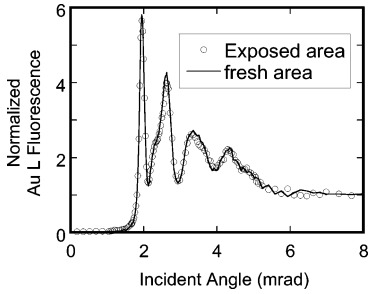

Figure 5. Damage check of a symmetric sandwich sample with $M = 350\,000$ after being annealed at 90 °C for 3 h (symbols). After the final scan of the measurement was finished, the sample was translated 2−3 mm, and a new scan was taken over an area of the sample that had not been exposed to the X-ray beam (solid line).

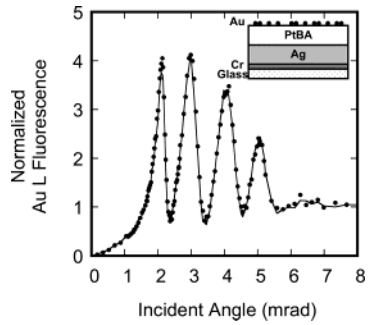

Figure 6. Normalized fluorescence for an open face sample with $M = 350\,000$ before (line) and after (symbol) annealing for 62 min at 100 °C.

only was there a slight shift to lower angles of the third and fourth fluorescence peaks, but there was also significant reduction of the amplitude modulation. The changes in the annealed profiles manifest themselves as increases in z_0 and σ. At the start of the anneal, there was an initial increase in z_0 of 20 Å that is at least partially due to thermal expansion as the temperature increased and approached the set point. The gold particle motions reported here correspond to motions that occurred after the temperature of the sample had reached the set point.

While under the He environment, radiation damage to the PtBA films at high temperature is reduced but may not be fully avoided. In addition, it has been shown that annealing of PtBA near 165 °C could cause degradation to occur. Therefore, annealing temperatures were kept below 110 °C, and at the end of each anneal a final measurement was performed on a new area that had not been exposed to the X-ray beam. Perfect overlap of this fluorescence profile with the final profile of the anneal was considered to be a sign of undamaged PtBA. An example comparison of this type is illustrated in Figure 5. All samples in this study were verified in this manner, and no detectable damage was found.

When the second PtBA layer was not added to the sample, resulting in "open-face" samples with the gold particles located at the surface of the film, no discernible particle motion was observed in the direction perpendicular to the surface of the film. This comparison is illustrated in Figure 6, which shows a comparison for the a gold layer at the surface of a 370 Å PtBA film with $M = 350\,000$, before and after a 62 min annealing treatment at 100 °C. These annealing conditions are more extreme than those used for the buried gold layer in Figure 4, for which motion of the gold particles was clearly observed. We expect PtBA to be able to form a

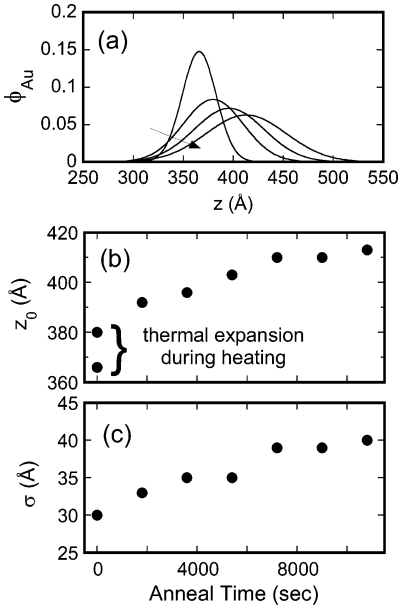

Figure 7. Gaussian distributions for symmetric sandwich with $M = 350\,000$ at room temperature and after annealing at 85 °C for 0, 60, and 150 min (a). The time dependence of z_0 (b) and σ (c) are also shown.

wetting layer on a clean gold surface, so we do not have an explanation for this result at this point.

The time evolution of the gold particle distribution during an annealing treatment for a symmetric sample (polymers with $w = 350\,000$ and equivalent thickness on each side of the gold layer) at 85 °C is illustrated in Figure 7. Two aspects of the time evolution of the gold particle distribution are evident from this picture. First, the center of the distribution moves away from the silver mirror toward the free surface of the polymer film. This effect, which we refer to as marker motion, is seen as an increase in z_0 with annealing time as shown in Figure 7b. The distribution also broadens over time, as described by the increase in the Gaussian width, σ, that is plotted in Figure 7c. In the following detailed discussion of these results, we begin with a treatment of the marker motion effect and follow this with a discussion of diffusive broadening of the particle distribution.

Marker Motion. Net motion of the entire gold particle distribution is attributed to an asymmetry in the polymer mobility for polymer molecules on either side of the gold layer. This asymmetry in the polymer mobility creates a net positive flux through the gold polymer layer that moves the particles toward the polymer layer with the higher mobility. The effect is similar to the marker motion experiments of Green et al., where the asymmetry in mobility was due to a molecular weight difference for the polymers on either side of the interface.[21] In our case, such an asymmetry in the mobility for the symmetric samples is due to the presence of the silver mirror and the air/film interface. Portions of molecules that are in direct contact with the silver mirror will have a decreased mobility as a result of interactions with this surface. If the bottom PtBA layer is sufficiently thin, then molecules in contact with the silver mirror will have portions of their segments extending to the layer of gold particles. The situation is illustrated by the plot in Figure 8, which shows ϕ_c, the local volume fraction corresponding to polymer molecules with at least one segment in contact with the substrate, as a function of distance away from the

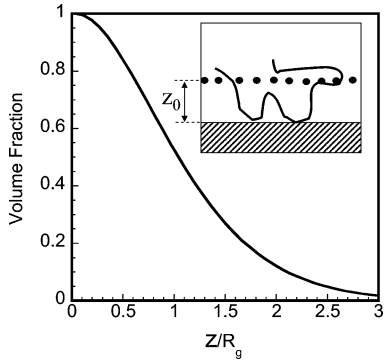

Figure 8. Local volume fraction of polymer segments corresponding to polymer molecules with at least one segment in contact with a solid surface located at $z = 0$. The inset shows the conformation of a single molecule that is in contact with the solid interface and with the gold particle layer located at $z = z_0$.

substrate. The curve was calculated numerically using a lattice model to describe the polymer chain statistics.[11]

A key parameter in our experiments is the normalized quantity z_0/R_g, the distance of the gold particle layer from the surface of the silver mirror divided by the polymer radius of gyration. While the chain dimensions of PtBA are not known in detail, we can assume that the characteristic ratio, C_∞, will be similar to that of polystyrene, since the phenyl group of polystyrene is similar in size and shape to the *tert*-butyl ester side chain of PtBA. Using the polystyrene value of 9.5[22] as a good estimate of C_∞ for PtBA, we obtain $R_g = 0.242M^{1/2}$ Å. For the data shown in Figure 7 we have $M = 350\,000$ and $z_0 = 380$ Å, giving $z_0/R_g = 2.65$. As illustrated in Figure 8, the fraction polymer segments in contact with the gold particle layer that correspond to polymer chains also in contact with the silver mirror is quite low; $\phi_c \approx 0.05$ for $z/R_g = 2.65$. Nevertheless, if this fraction of chains are hindered in their motions, it may be sufficient to give the marker motion that is observed because motions of polymer molecules in the top layer are not at all hindered. Preliminary results from other samples indicate that marker motion is reduced substantially by increasing z_0/R_g, by either increasing the thickness of the bottom PtBA layer or decreasing the molecular weight.

The data plotted in Figure 7 are from "symmetric" samples, where the PtBA layers on either side of the gold layer had the same molecular weight. To investigate the relationship between marker motion and diffusive broadening in more detail, two "asymmetric" samples were also made, where the molecular weights of the two 375 Å PtBA layers were different. The molecular weights of the two samples were 350 000 and 185 000, and the samples are denoted Ag/350/185 and Ag/185/350. As the names imply, the Ag/350/185 sample has the higher molecular weight polymer as the bottom layer in contact with the silver mirror, whereas the Ag/185/350 has the lower molecular weight polymer in contact with the silver mirror. The fluorescence profiles for the two unannealed samples are identical and are illustrated in Figure 9a. Significant changes are observed after annealing for 30 min at 100 °C, as illustrated in parts b and c of Figure 9.

The gold distributions obtained from the fits to the fluorescence profiles are shown in Figure 10. The value of z_0 increases by about 20 Å when the room temperature sample is increased from room temperature to

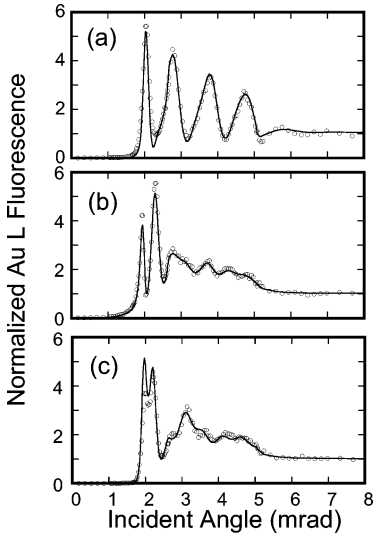

Figure 9. Fluorescence profiles for asymmetric samples where the two polymer layers had different molecular weights. Solid lines are fit the data, using the Gaussian profiles of eq 3. (a) Room temperature scan, which was nearly identical for each of the two samples ($z_0 = 375$ Å and $\sigma = 19$ Å). (b) Ag/350/185 sample after 30 min at 100 °C ($z_0 = 564$ Å and $\sigma = 58$ Å). (c) Ag/185/350 sample after 30 min at 100 °C ($z_0 = 290$ Å and $\sigma = 50$ Å).

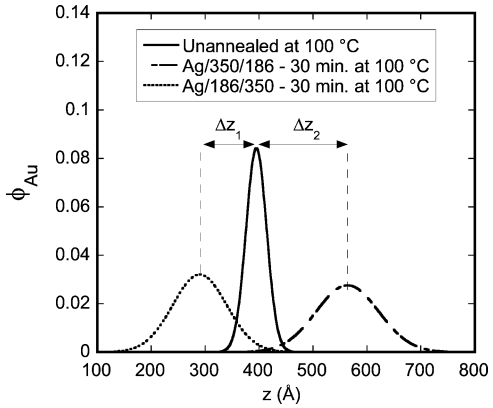

Figure 10. Gold distribution for asymmetric samples used to generate the fits plotted in Figure 9. The value of z_0 for the unannealed samples has been increased from 375 to 395 Å to account for thermal expansion as the sample is heated from room temperature to 100 °C.

100 °C, and this increase has been accounted for in the unannealed profile in Figure 10. The effects of the annealing treatment are to broaden the gold particle distribution and to shift the center of the distribution toward the polymer with the lower molecular weight; i.e., z_0 increases during annealing for the Ag/350/185 sample and decreases for the Ag/185/350 sample. Utilizing the analysis of Green et al.,[21] we can obtain D_A^*, the tracer diffusion coefficient for the polymer with $M = 185\,000$, from the following expression:

$$\Delta z = C(D_A^* t)^{0.5} \tag{7}$$

where Δz is the shift in the position of the gold layer, t is the annealing time, and C is a factor that depends on the ratio of the tracer diffusion coefficients for the two polymers. For entangled polymer chains diffusing by reptation, C depends only on the molecular weight ratio and is equal to 0.27 in our case.[21] As illustrated in Figure 10, $\Delta z = \Delta z_1 = 105$ Å for the Ag/185/350

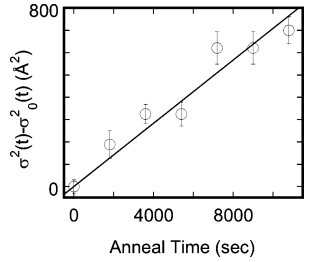

Figure 11. Determination of the diffusion coefficient from the data plotted in Figure 7c. The solid line corresponds to a diffusion coefficient of 3.5×10^{-18} cm^2/s, calculated according to eq 8.

sample and $\Delta z = \Delta z_2 = 169$ Å for the Ag/350/185 sample. Using these values for Δz, eq 7 gives $D_A^* = 8.4 \times 10^{-15}$ cm^2/s when the low molecular weight polymer forms the bottom layer, and $D_A^* = 2.2 \times 10^{-14}$ cm^2/s when this polymer is used as the top layer.

These estimates of D_A^* invoke the assumption that the diffusion coefficients of both polymers are independent of both local composition and position. The composition dependence for these relative molecular weights is not expected to be very strong,[23] but a depth dependence is obviously observed. When the low molecular weight polymer layer is in contact with the silver mirror, its mobility is decreased, thereby decreasing the mobility contrast that is responsible for the change in z_0. When the low molecular weight polymer is at the free surface, this mobility contrast is increased, and z_0 changes more rapidly with time. In the absence of these surface effects, the measured value of D_A^* is expected to lie between the two values reported above. These marker motion experiments are, in fact, a very sensitive probe of the interfacial dynamics in these thin polymer films. More thorough investigations of the time dependence of the marker motion and of the effects of molecular weight and thickness of the bottom layer are required to study these issues more quantitatively.

Diffusive Broadening of the Gold Particle Distribution. Brownian diffusion of the gold particles themselves can be quantified by an analysis of the time dependence of the Gaussian width, σ. The time dependence of the interfacial broadening can be used to define a particle diffusion coefficient, D_{Au}, through the following relationship:

$$\sigma^2(t) = \sigma_0^2 + 2D_{Au}t \tag{8}$$

where σ_0 is the value of σ at a point near the beginning of the annealing treatment, where t is defined to be zero. Data from Figure 7c are plotted this way in Figure 11 and give a value of 3.5×10^{-18} cm^2/s for D_{Au}. Measured values of the diffusion coefficient at different temperatures for samples with $M = 100\,000$ and $M = 350\,000$ are plotted in Figure 12. Values obtained from the particle broadening in the asymmetric samples are also shown in Figure 12. In this case it is interesting to note that the diffusion coefficient of the gold particles themselves obtained from the particle broadening ($\approx 7 \times 10^{-17}$ cm^2/s) is much less than the diffusion coefficient of the lower molecular weight polymer in the asymmetric diffusion couple ($\approx 10^{-14}$ cm^2/s). This large difference in the diffusion coefficients for the polymer and the particles themselves is an important property of this system that makes the marker motion experiments

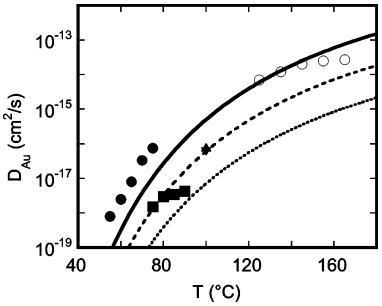

Figure 12. Gold particle diffusion coefficient as a function of annealing temperature. $M = 100\,000$ (○) from RBS measurements (ref 11); symmetric samples with $M = 100\,000$ (●) and $M = 350\,000$ (■) from XSW measurements. The asymmetric molecular weight cases are also shown for the Ag/350/185 (▲) and Ag/185/350 (▼) samples. Lines represent fits to eq 9, with $\Delta = 2.3$ Å and $M = 100\,000$ (—), $M = 185\,000$ (- - -), and $M = 350\,000$ (···).

Table 1. Values of the Effective Diffusive Step Length (Δ) and the Effective Hydrodynamic Radius (*R*) for a Gold Particle Layer with *z = 4 Å, Confined between PtBA Layers Having the Molecular Weights Indicated**

M (top)	*M* (bottom)	Δ (Å)	*R* (Å)	method[a]
100 000	100 000	2.3	≈3000	RBS
100 000	100 000	6	≈400	XSW
185 000	350 000	2.5	≈3000	XSW
350 000	185 000	2.5	≈3000	XSW
350 000	350 000	5	≈600	XSW

[a] RBS = Rutherford backscattering spectrometry (from ref 11); XSW = X-ray standing waves.

feasible, since the gold peak remains narrow enough so that the shift in its location can be accurately determined.

For discussion purposes, it is useful to define an effective diffusive step size Δ, which is temperature independent. The diffusion coefficient is determined by the step size and the relaxation time in the following manner:

$$D_{Au} \equiv \frac{\Delta^2}{6\tau} = 1.15 \times 10^7 M^{-3.4} \Delta^2 \exp(-1626/(T + 16)) \quad \text{cm}^2/\text{s} \tag{9}$$

with Δ in Å, T in °C, and M in g/mol. The predictions of eq 9 for $\Delta = 2.3$ Å are shown on Figure 12 for $M = 100\,000$, 185 000, and 350 000. The diffusion results can also be described by using the Stokes−Einstein equation to define an effective radius, R, of the diffusing particles, i.e., $D_{Au} = k_B T/6\pi\eta_0 R$. From the definition for Δ given in eq 9, we obtain the following relationship between Δ and R:

$$R = \frac{k_B T}{\pi \Delta^2 G_n^0} \tag{10}$$

Values of Δ and R obtained by fitting eqs 9 and 10 to the measured values of D_{Au} are listed in Table 1. For the asymmetric molecular weight samples, the lower value of M was used to calculate Δ from eq 9. It is evident from these results that diffusive particle motions over these short length scales are coupled to the bulk relaxation times of the entanglement network, even though the diffusion distances and metal particle sizes are smaller than the entanglement mesh size, equal to about 100 Å for PtBA. As a result, the gold

particle diffusion coefficients remain highly molecular weight dependent, with values of Δ that are roughly constant for the few entangled polymer systems that we have been able to study. Despite this general coupling to τ, we do observe slightly faster diffusion at the short times than at longer times. Over long times, the gold particle distribution reorganizes within the plane of the film, so it is not surprising that the diffusive dynamics in the direction perpendicular to the film surface evolve with time.

The low values of the Δ, or, equivalently, the relatively large values of R, are not consistent with the diffusion of "noninteracting" particles in a viscous polymer matrix. This is especially true since the particle size itself is less than the mesh size of the entanglement network of the polymer matrix. Consider, for example, the tracer diffusion of relatively low molecular weight polymers in a high molecular weight polymer matrix that is chemically equivalent. If the coil sizes of the tracer molecules are less than the entanglement mesh size of the matrix, the tracer diffusion is no longer coupled to the entanglement lifetime.[24] In effect, these small tracer polymers are able to diffuse through the entanglement network in an unimpeded fashion. The gold particles in our system cannot be viewed as "inert" or "noninteracting" in the same sense that these tracer polymer molecules can be viewed as inert. The physical picture is that of a "transient" network, where the individual gold particles can be viewed as cross-link points that have a finite lifetime. The picture is valid when the average distance between gold particles is less than the typical dimensions of a polymer molecule, a picture that has been quantified in more detail previously.[11] The lifetime of these effective network points is coupled to the exchange kinetics of polymer segments at the polymer/gold interface. The net effect of this exchange process is to increase the effective relaxation time of the polymer matrix, thereby decreasing the gold polymer diffusion coefficient. The effective step size, Δ, decreases as well, since this quantity is defined in terms of the relaxation time of the polymer in the absence of the gold. A new result contributed by the XSW results is that this model provides a consistent method for analyzing diffusive motions of the particles even when the length scale of these motions is less than the characteristic length scale of the entanglement network itself.

Conclusions

The results obtained from the XSW measurements indicate that diffusion motions of the gold particles are coupled to the terminal relaxation time of the polymer film. For $t \approx \tau$, particles diffuse over distances equal to a relatively small fraction of the tube diameter. An important consequence of this result is that particle diffusion over short length scales in more complicated morphologies, such as the ordered diblock morphologies mentioned in the Introduction, may be exceptionally slow because of the very long relaxation times in these systems.

A second result concerns the effect of the substrate on the diffusion of the gold particles themselves. An asymmetry of the polymer mobility on either side of the gold particle layer drives the particles toward the high mobility side. Effects of the silver substrate on the mobility of the PtBA chains result in a net driving force for the gold particle layer to move toward the free surface.

Acknowledgment. Participation of S. Cheong and A. Richter, and technical support by the 1-BM staff at the APS is greatly appreciated. The authors thank M. Bedzyk for valuable discussions. Use of the APS and this work were supported by the U.S. Department of Energy, Office of Science, Office of Basic Energy Sciences, under Contract W-31-109-ENG-38. We also thank Prof. W. R. Burghardt with assistance with the rheometry.

References and Notes

(1) Spatz, J. P.; Roescher, A.; Moller, M. *Adv. Mater.* **1996**, *8*, 337.
(2) Spatz, J. P.; Mossmer, S.; Hartmann, C.; Moller, M.; Herzog, T.; Krieger, M.; Boyen, H. G.; Ziemann, P.; Kabius, B. *Langmuir* **2000**, *16*, 407.
(3) Mossmer, S.; Spatz, J. P.; Moller, M.; Aberle, T.; Schmidt, J.; Burchard, W. *Macromolecules* **2000**, *33*, 4791.
(4) Morkved, T. L.; Wiltzius, P.; Jaeger, H. M.; Grier, D. G.; Witten, T. A. *Appl. Phys. Lett.* **1994**, *64*, 422.
(5) Zehner, R. W.; Lopes, W. A.; Morkved, T. L.; Jaeger, H.; Sita, L. R. *Langmuir* **1998**, *14*, 241.
(6) Thurn-Albrecht, T.; Schotter, J.; Kastle, C. A.; Emley, N.; Shibauchi, T.; Krusin-Elbaum, L.; Guarini, K.; Black, C. T.; Tuominen, M. T.; Russell, T. P. *Science* **2000**, *290*, 2126.
(7) Lin, B. H.; Morkved, T. L.; Meron, M.; Huang, Z. Q.; Viccaro, P. J.; Jaeger, H. M.; Williams, S. M.; Schlossman, M. L. *J. Appl. Phys.* **1999**, *85*, 3180.
(8) Weber, R.; Zimmermann, K. M.; Tolan, M.; Stettner, J.; Press, W.; Seeck, O. H.; Erichsen, J.; Zaporojtchenko, V.; Strunskus, T.; Faupel, F. *Phys. Rev. E* **2001**, *64*, 061508.
(9) Lopes, W. A.; Jaeger, H. M. *Nature (London)* **2001**, *414*, 735.
(10) Cole, D. H.; Shull, K. R.; Rehn, L. E.; Baldo, P. *Phys. Rev. Lett.* **1997**, *78*, 5006.
(11) Cole, D. H.; Shull, K. R.; Baldo, P.; Rehn, L. *Macromolecules* **1999**, *32*, 771.
(12) Ahn, D.; Shull, K. R. *Macromolecules* **1996**, *29*, 4381.
(13) Varshney, S. K.; Jacobs, C.; Hautekeer, J. P.; Bayard, P.; Jerome, R.; Fayt, R.; Teyssie, P. *Macromolecules* **1991**, *24*, 4997.
(14) Ohring, M. *The Materials Science of Thin Films*; Academic Press: San Diego, 1992.
(15) Batterman, B. W. *Phys. Rev. Lett.* **1969**, *22*, 703.
(16) Golovchenko, J. A.; Patel, J. R.; Kaplan, D. R.; Cowan, P. L.; Bedzyk, M. J. *Phys. Rev. Lett.* **1982**, *49*, 560.
(17) Andersen, S. K.; Golovchenko, J. A.; Mair, G. *Phys. Rev. Lett.* **1976**, *37*, 1141.
(18) Bedzyk, M. J.; Bommarito, G. M.; Schildkraut, J. S. *Phys. Rev. Lett.* **1989**, *62*, 1376.
(19) Wang, J.; Caffrey, M.; Bedzyk, M. J.; Penner, T. L. *Langmuir* **2001**, *17*, 3671.
(20) Parratt, L. G. *Phys. Rev.* **1954**, *95*, 359.
(21) Green, P. F.; Palmstrom, C. J.; Mayer, J. W.; Kramer, E. J. *Macromolecules* **1985**, *18*, 501.
(22) Boothroyd, A. T.; Rennie, A. R.; Wignall, G. D. *J. Chem. Phys.* **1993**, *99*, 9135.
(23) Green, P. F.; Kramer, E. J. *Macromolecules* **1986**, *19*, 1108.
(24) Richter, D.; Willner, L.; Zirkel, A.; Farago, B.; Fetters, L. J.; Huang, J. S. *Macromolecules* **1994**, *27*, 7437.

MA0486593